Available online at www.sciencedirect.com
SCIENCE DIRECT®
Polymer 45 (2004) 1833–1843
polymer
www.elsevier.com/locate/polymer

Atomic force microscopy study of comb-like vs. arborescent graft copolymers in thin films

Pascal Viville[a,*], Philippe Leclère[a], Alain Deffieux[b], Michel Schappacher[b], Julien Bernard[b], Redouane Borsali[b], Jean-Luc Brédas[a,c], Roberto Lazzaroni[a]

[a]*Service de Chimie des Matériaux Nouveaux, Centre de Recherche en Sciences des Matériaux Polymères (CRESMAP), Université de Mons-Hainaut 20, Place du Parc, 7000 Mons, Belgium*
[b]*Laboratoire de Chimie des Polymères Organiques, UMR ENSCPB-CNRS 5629, Universit de Bordeaux, 16 Avenue Pey Berland 33607 Pessac, France*
[c]*Department of Chemistry, The University of Arizona, Tucson, AZ 85721-0041, USA*

Received 19 February 2003; received in revised form 5 January 2004; accepted 12 January 2004

Abstract

This work deals with the study of comb-like vs. arborescent grafted copolymers made of poly(chloroethyl vinyl ether)-*g*-polystyrene (PCEVE-*g*-PS). We describe how the molecular architecture of the branched polymers affects their nanoscale organization in thin films, as observed using atomic force microscopy. The results indicate that modifying the molecular architecture from a 'generation-zero' comb-like (PCEVE-*g*-PS) to a 'first-generation' hyperbranched (PCEVE-*g*-(PS-*b*-PCEVE-*g*-PS)) architecture strongly modifies the observed geometrical parameters of the molecules, in good agreement with the expected evolution of the molecular dimensions and the corresponding data obtained in solution.

The surface organization of the (PCEVE-*g*-PS) copolymer molecules is also strongly conditioned by the interplay between the molecule–substrate interactions and the molecule–molecule interactions, leading to different possible orientations of the lateral branches with respect to the surface and thus to different final morphologies.

Keywords: Atomic force microscopy; Thin films; Hyperbranched

1. Introduction

An important challenge in polymer-based advanced materials aimed at the fabrication of nanoscale devices relies on the development of new synthetic routes allowing the design of specific molecular architectures that can, in turn, self-arrange into well-organized molecular assemblies. Such bottom–up approach can provide a new route for the fabrication of nanometer-size periodic structures with a well-controlled morphology, that could be of interest in many industrial and technological applications [1–6]. Recent progress in polymer chemistry have allowed one to generate new polymer materials with tailored molecular architectures and dimensions. For instance, intense research activity has been recently devoted to the synthesis of highly-specific branched and hyperbranched polymers with dendritic, dendronized, star- and comb-like architectures [7–17]. Branched polymers exhibit bulk and solution physical properties that can be very different from those of their linear homologs. For instance, they possess a large number of terminal functional groups and an intrinsic globular structure that can lead to specific rheological properties [11,17–19]. Compared to dendrimers, hyperbranched macromolecules are characterized by a lower degree of branching, a less perfect architecture, but still possess a nonlinear molecular architecture and a very high number of potentially reactive end groups. They can be prepared much more rapidly and economically than dendrimers (in a reduced number of synthetic steps) and are therefore considered as interesting alternatives to dendrimers in a number of applications [5,11,20]. Last but not least, thanks to their specific molecular architecture, hyperbranched polymers are good candidate materials to form well-organized assemblies [5,6].

Recently, a new route for the preparation of well-controlled

* Corresponding author. Tel.: +32-65-373-868; fax: +32-65-373-861.
E-mail address: pascal@averell.umh.ac.be (P. Viville).

0032-3861/$ - see front matter © 2004 Elsevier Ltd. All rights reserved.
doi:10.1016/j.polymer.2004.01.030

comb-like and hyperbranched architectures has been proposed. The method is based on the synthesis of branched poly(chloroethyl vinyl ether-*g*-styrene) (PCEVE-*g*-PS) copolymers through the grafting reaction of polystyryl lithium segments onto poly(chloroethyl vinyl ether) chains [14,21–23]. This approach offers several advantages compared to other methods. First, the selectivity of the coupling reaction is very high and allows for complete substitution of the chloride groups of the initial CEVE units by PS chains, thus allowing the synthesis of well-defined comb-like polymers. Moreover, the living polymerization techniques used allow the control of the dimensions of the grafted PS branches and the PCEVE main backbone, so that both the length and the number of branches of the graft copolymers can be tuned. As a consequence, different degrees of molecular architecture complexity can be generated and various molecular assemblies can be expected to occur.

In this work, we investigate the nanoscale organization of these new branched (PCEVE-*g*-PS) copolymer molecules in thin solid films. For that purpose, we use atomic force microscopy (AFM) to probe the surface topography with very accurate lateral resolution. In recent studies, AFM has been shown to be a powerful technique to study the morphology of similar comb-like (or brush-like) polymer molecules and to determine their molecular characteristics, such as absolute molar mass, molar mass distribution and chain conformation [13,15,24–27]. For instance, these studies have demonstrated that comb-like polymers can change their conformation from statistical coils to wormlike cylindrical brushes, because of the steric hindrance due to the lateral segments. Depending on the density of branches, the stiffness of the chain is modified; in a situation where the branch density is high, the steric repulsion between the side chains leads to stiffening of the backbone, the persistence length then becoming comparable to the contour length. This effect has also been theoretically predicted based on scaling concepts [28] and using mean-field analytical approaches [29] and Monte Carlo simulations [30,31].

In that context, we aim at understanding how the molecular architecture of (PCEVE-*g*-PS) copolymer molecules affect their dimensions, i.e. their size and shape and organization on surfaces. For that purpose, we consider here (PCEVE-*g*-PS) copolymers with very high molar masses, which facilitates the direct observation of individual molecules by AFM. We focus on the influence of the side-chain complexity on the dimensions and organization of the molecules, starting from a comb-like (generation zero) structure (PCEVE-*g*-PS) and going to a more complex (first-generation) hyperbranched structure (PCEVE-*g*-(PS-*b*-(PCEVE-*g*-PS)).

We also address the fundamental question of how the interactions between the substrate and the copolymer molecules affect their surface positional and orientational order by changing the nature of the substrate, i.e. hydrophobic vs. hydrophilic.

2. Experimental section

Synthesis of comb-like and arborescent graft polystyrene (Fig. 1). A poly(chloroethyl vinyl ether)(PCEVE) (a), $\overline{DP}_n = 760, \bar{M}_w/\bar{M}_n = 1.03$, is first synthesized as previously described by living cationic polymerization of chloroethyl vinyl ether using propyl diethylacetal/trimethylsilyl iodide as initiating system and zinc chloride as catalyst and used as reactive backbone [14]. Then living ω-diethylacetal polystyryl lithium chains (b), $\overline{DP}_n = 80$, are prepared using propyl lithium diethylacetal as initiator and grafted onto the PCEVE backbone (a) to form a comb polymer with ω-diethylacetal polystyrene branches (I). The grafting reaction is achieved by adding the living PSLi solution onto a known quantity of PCEVE in benzene solution [7]

The molar mass of the obtained PS comb, experimental $\bar{M}_n = 7.7 \times 10^6$ g/mol, $\bar{M}_w/\bar{M}_n = 1.06$, was determined using elastic light scattering and found close to the theoretical value (e.g. 6.5×10^6 g/mol) calculated assuming one PS graft per chloroethyl vinyl ether unit, in agreement with a quantitative grafting reaction. The dimensional characteristics are collected in Table 1.

In a second step, the PCEVE-*g*-(ω-diethylacetal PS) comb polymer (I) is used as a macro-pluri-initiator to grow from the end of each diethylacetal PS branch a new PCEVE

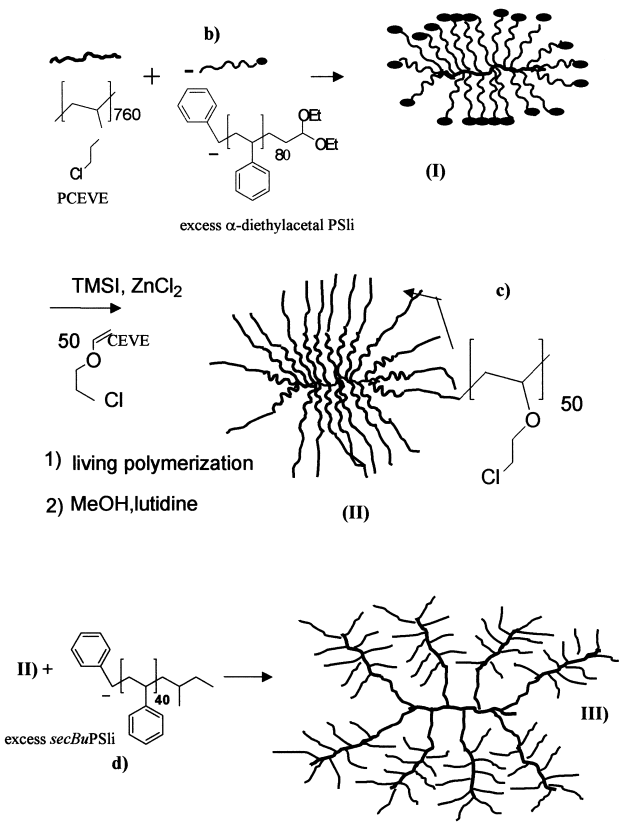

Fig. 1. Reaction scheme for the synthesis of comb-like (PCEVE-*g*-PS) and first-generation hyperbranched (PCEVE-*g*-(PS-*b*-(PCEVE-*g*-PS)) grafted copolymers.

Table 1
Typical dimensional and solution characteristics of (760/80) (PCEVE-*g*-PS) comb-like and (760/80/50/40) (PCEVE-*g*-(PS-*b*-(PCEVE-*g*-PS)) hyperbranched copolymer molecules

Constitutive blocks ($\overline{DP}_n$)	$\overline{Mn}_{th}$ 10^{-6}	$\bar{M}n_{app}$ [a] SEC (RI) 10^{-6}	$\overline{Mw}_{exp}$ [b] (LS) 10^{-6}	$\bar{M}_w/\bar{M}_n$	$[\eta]$ [c] (dl/g)	R_h [d] (nm)	R_g [e] (nm)	R_g/R_h
760–80	6.5	0.99	7.7	1.06	0.46	47.4	52.9	1.12
760–80–50–40	150.0	3.10	98	1.13	0.19	67.8	82.8	1.22

[a] Determined by SEC using PS standards.
[b] Determined by elastic light scattering in THF.
[c] Measured at 25 °C in THF.
[d] Determined from dynamic light scattering measurements.
[e] Determined from elastic light scattering measurements.

block (c), $\overline{DP}_n = 50$. As in the first step living CEVE polymerization is initiated by addition of trimethylsilyl iodide to convert the acetal termini into iodoether groups and zinc chloride as catalyst. The corresponding PCEVE-*g*-(PS-*b*-PCEVE) comblike copolymer (II) (experimental $\bar{M}w = 1.5 \times 10^6$g/mol, $\bar{M}_w/\bar{M}_n = 1.06$, (determined using elastic light scattering) is purified by selective precipitation from free PCEVE chains. It is then used as new reactive backbone for grafting a second set of ω-diethyl acetal PSLi chains (d), $\overline{DP}_n = 40, \bar{M}_w/\bar{M}_n = 1.03$, to finally yield ω-diethyl acetal functionalized polystyrene dendrigraft PCEVE-*g*-(PS-*b*-(PCEVE-*g*-diethylacetal PS)) (III). Due to the large difference in their molar masses, the hyperbranched polymer can be easily separated from free ω-acetal polystyrene by selective reprecipitation into a hydrocarbon mixture. The dimensional characteristics are collected in Table 1.

The molar masses were measured by SEC using both refractive index (RI) and light scattering detectors (LS) and the gyration and hydrodynamic radius were determined respectively by elastic and dynamic light scattering in THF at 25 °C.

The molecular architectures investigated in this work are shown in Fig. 2. They consist of one (PCEVE-*g*-PS) comb-like architecture, namely the (760/80) copolymer. To compare with comb-like architectures, we also studied a copolymer with a (760/80/50/40) (PCEVE-*g*-(PS-*b*-(PCEVE-*g*-PS)) hyperbranched architecture.

Samples for AFM analysis were prepared by solvent casting at ambient conditions starting from solutions in tetrahydrofuran (THF), which is a good solvent for PS. Typically, 20 μl of a dilute solution (from 10^{-4} up to 0.1 wt%) was cast on a 1×1 cm^2 freshly-cleaved mica or highly oriented pyrolytic graphite (HOPG) substrate. Samples were analyzed after complete evaporation of the solvent at room temperature and after a 24 h annealing of the samples at 120 °C (above the (PCEVE-*g*-PS) glass transition temperature (99 °C) in 10^{-6} Torr vacuum. Annealing was carried out in order to improve the surface ordering of the molecules and to approach the thermodynamic equilibrium of the deposits.

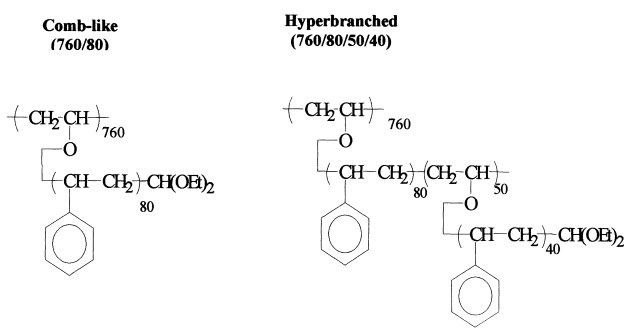

Fig. 2. Molecular architectures of the comb-like and hyperbranched (PCEVE-*g*-PS) copolymers studied in this work.

All AFM images were recorded in air with a Nanoscope IIIa microscope operated in tapping mode (TM) [32]. The probes are commercially available silicon tips with a spring constant of 24–52 N/m, a resonance frequency lying in the 264–339 kHz range and a typical radius of curvature in the 10–15 nm range. In this work, both the topography and the phase signal images were recorded with the highest sampling resolution, i.e. 512×512 data points.

3. Results and discussion

Deposits on mica from dilute solutions (0.01 wt%) do not generate homogeneous continuous films but rather layered surface patterns that originate from the dewetting of the polymer solution from the mica substrate during the drying process (Fig. 3). A cross-section analysis of the structures (for instance; along the black dashed line in the image of Fig. 3) reveals areas that exhibit the same height. The analysis also reveals that the brighter areas have twice the height of the gray zones: the gray areas correspond to a flat, 7 ± 0.6 nm-thick, layer of the (760/80) copolymer while the brightest zones are 14 ± 0.5 nm-thick deposits. As the dewetting proceeds further, thicker deposits are locally formed, with a thickness of 21 ± 0.6 nm. In our height measurements, the magnitude of the tip–sample interactions, defined in TM–AFM by the ratio between the setpoint amplitude (A_{sp}) and the amplitude of the free-oscillating cantilever (A_0) was lowered as much as possible ($A_{sp}/A_0 \cong 1$; i.e. very close to the tip disengagement from the sample) [32]. This was carried out in order to minimize the loading force applied to the sample during imaging and,

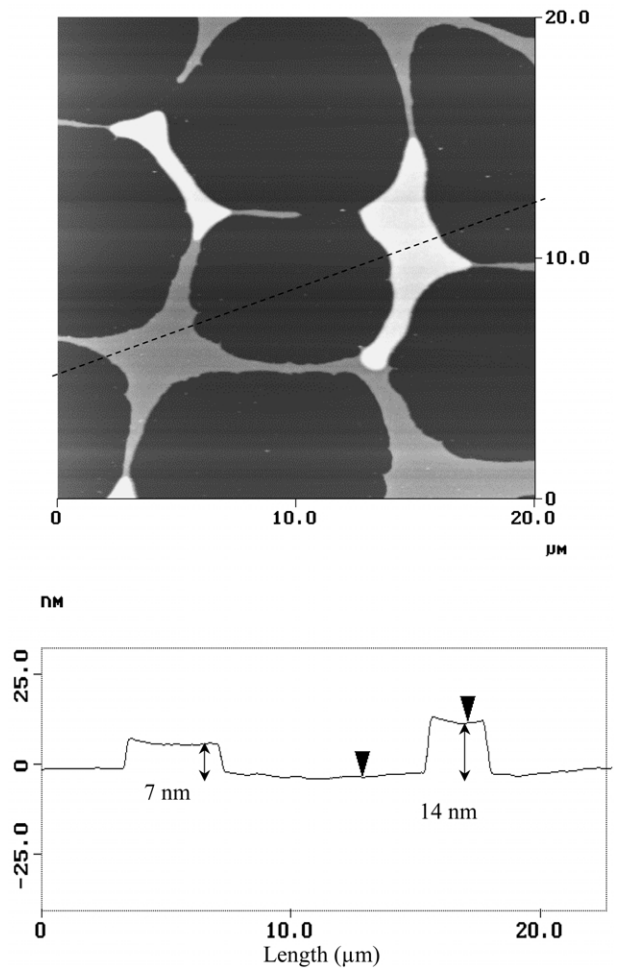

Fig. 3. Left: TM–AFM topographic image ($20 \times 20\ \mu m^2$) of the multilayer organization for the (760/80) copolymer prepared from a 0.01 wt% solution. The vertical scale is 25 nm. Right: cross-sectional analysis.

therefore, to avoid the squeezing of the material between the tip and the substrate. Under these conditions, the measurement of the height of the features in the images is reliable. The multiplicity observed in the height of the layers, and the fact that no feature thinner than 7 nm has been observed, suggests that the 7 nm-thick layer represents a monolayer of the (760/80) copolymer. The thicker deposits thus correspond to bilayers and trilayers.

This multilayered morphology of the deposits on mica was observed for all investigated copolymer compositions. As an illustration, Figs. 5 and 6 show high magnification images of the (760/80) and the (760/80/50/40) copolymer monolayers generated by casting on mica, after the samples have been annealed for 24 h at 120 °C. The cross-section analysis of these images shows that the two copolymer monolayers are different in height, (760/80/50/40) copolymer monolayers being much thicker than (760/80) monolayers: 26 ± 0.7 vs. 7 ± 0.6 nm, respectively. This result shows that a change in copolymer molecular architecture strongly affects the thickness of the corresponding monolayers and thus, the height of the molecules within the monolayers. This evolution in the height of the molecules is to be expected when considering the important increase of the steric hindrance of the side chains in the case of the hyperbranched (760/80/50/40) copolymer.

The images in Figs. 5 and 6 also show that the monolayers are organized into densely-packed molecules. Fig. 7 better illustrates this organization by comparing higher magnification TM–AFM phase images of the (760/80) and the (760/80/50/40) copolymer monolayers. These images clearly show that the monolayers are characterized by a well-defined internal morphology at the nanometer scale, made of long molecules assembled parallel to each other, along with regions where the molecules fold (for instance, the bright feature marked by an arrow in the left image). In agreement with the results of recent works [27], such a morphology originates from the intrinsic comb-like molecular architecture of the copolymers that forces the macromolecules to adopt a conformation of wormlike cylindrical brushes. As an illustration, a sketch of a cylindrical brush is shown as the left inset in Fig. 7. In the present case, the cylindrical brush conformation is induced by the large steric hindrance caused by the presence of the PS grafted segments that increase the stiffness of the main PCEVE backbone. The intermolecular ordering observed in the images of Fig. 7 is controlled by the steric repulsion between the grafted PS chains, which means that the distance between two neighboring molecules in the images corresponds to the distance between the centre of two neighboring PCEVE backbones (central inset in Fig. 7). In most AFM images, the molecules appear as continuous objects within which interruptions are discernable. Considering that these interruptions are chain ends, we can evaluate the total contour length (L_{tot}) of the molecules. For that purpose, a large number of individual chains, taken from different representative TM–AFM images, are digitalized by means of a picture analysis routine allowing to export these chains as a succession of pixels whose coordinates are then analysed. Contour length L_{tot} is then calculated as the sum of the different elemental segment lengths constituting one chain, following a method described in Ref. [33]. Following this procedure, we could determine the experimental L_{tot} for a large number of molecules of the comb-like and the arborescent copolymer. Considering that the molecular mass is proportional to the contour length (L_{tot}) of the molecules, it was then possible to determine the molecular length distribution, as for a molecular mass distribution obtained from SEC measurements. Fig. 8 shows the molecular length distribution obtained in the case of the comb-like (760/80) copolymer. The number average molecular (L_n) and the length average molecular (L_w) length values, both determined from that distribution, are found to be 176 and 179 nm, respectively. It is worth noting here that the distribution is very narrow; the polydispersity index of the molecular length obtained from AFM images ($L_w/L_n = 1.02$) is in very good agreement with the one determined from SEC measurements

($M_w/M_n = 1.06$). The molecular length distribution for the arborescent species (not shown here) yields an equivalent value for L_n, consistent with the same DP value of its main PCEVE backbone. Considering, as an extreme case, that a fully extended PCEVE backbone with 760 monomer units yields a theoretical value of ~190 nm for the main chain contour length, we conclude that the objects appearing in the two images of Fig. 7 are indeed single molecules.

On that basis, an important information revealed by the two TM–AFM images in Fig. 7 is the huge increase in the width of the molecules when the structural complexity of the lateral side chain is modified from that of a comb-like (760/80) to a first generation hyperbranched (760/80/50/40) copolymer. The large increase in the molecule width observed for the (760/80/50/40) composition is explained by the fact that, in this case, each lateral segment of the molecule consists of a comb-like structure itself, bound to a common backbone (see right inset in Fig. 7). The higher steric hindrance of these longer and bulkier side chains causes the average width of the molecules to increase from 13 ± 0.7 nm for the (760/80) copolymer up to 40 ± 1.1 nm for the (760/80/50/40) copolymer.

This evolution is completely consistent with the evolution of the corresponding molar masses measured in solution by elastic light scattering (i.e. $M_w = 7.7$ and 98×10^{-6} g/mol for the comb and the arborescent, respectively). In particular, we have calculated the ratio between the molecular volumes of the comb and the arborescent molecules on the basis of the dimensions obtained from the AFM images (i.e. $V_{arborescent}/V_{comb} = 11.4$). This ratio is almost identical to the ratio between the corresponding experimental molecular masses given in Table 1 ($M\mathrm{w}_{arborescent}/M\mathrm{w}_{comb} = 12.7$). This clearly shows that the variation of the lateral dimensions observed by AFM is consistent with that of the molecular masses.

As it can be seen in Table 1, the experimental molar mass of (760/80) determined using elastic light scattering is in good agreement with the calculated theoretical molar mass assuming an almost full substitution of chloride of CEVE by PS chains. In the case of (760/80/50/40), a lower grafting efficiency is however observed ($\overline{M\mathrm{w}}_{exp} = 98 \times 10^6$ g/mol and $\overline{M\mathrm{n}}_{th} = 150 \times 10^6$ g/mol) suggesting that PS grafting on the PCEVE branches of the (760/80/50/40) was not complete. The low $\bar{M}_n$ values measured by SEC (RI) for the two structures are consistent with the highly branched architecture of the copolymers. Static and dynamic light scattering measurements allowed us to determine respectively R_g and R_h (see Fig. 4). The ratio $\rho = R_g/R_h$ which is a sensitive fingerprint of the macromolecule shape and compacity varies from 1.12 for (760/80) to 1.22 in the case of (760/80/50/40). These ρ values are very similar to those reported by Antonietti [34] ($\rho = 1.03–1.30$) and Liu [35]. ($\rho = 1.15–1.22$) for cylindrical micelles and agree with the shapes observed by AFM. It is worth noting that worm-like or cylindrical molecules should present a value $\rho \gg 1.85$, value for linear coiled chain in good solvent. This value of course assumes that the diameter is negligible as compared to the length of the molecule. For comb-like and hyperbranched molecules, however, such a value cannot hold for simple geometrical arguments: indeed the diameter of such molecules is not any more negligible and its contribution to the R_g and R_h tends to break the balance between thermodynamic and hydrodynamic interactions. This simple geometrical conformation should lead to a decrease of ρ. In another words, for the same molar mass, the hyperbranched molecule could have a spherical geometry while the equivalent simple comb-like with small branches could be worm-like shaped. That why most of the studied systems report a low value of ρ (e.g. ranging from 1 to 1.3).

One intriguing characteristic of the AFM images of Figs. 5 and 6 is the fact that both comb and hyperbranched molecules tend to orientate perpendicularly to the borderline of monolayers. This effect is particularly well illustrated in the images of the hyperbranched copolymer monolayers (Fig. 6B); indeed, in this case, one can even observe certain molecules that coil in order to expose their two extremities towards the border of the monolayer. We believe that such orientation is driven by the capillary forces arising at the contact between the molecules and the drying solvent, during the radial contraction of the droplets.

An important aspect which is worth noting at this stage is that the molecules that are organized within monolayers (Figs. 5–7) have different height and width. This is observed for the two copolymer compositions. We recall that, in the case of the (760/80) copolymer, the width of a molecule within one monolayer is 13 ± 0.7 nm while its height is 7 ± 0.6 nm. The (760/80/50/40) copolymer molecules exhibit a width of 40 ± 1.1 nm and a height of 26 ± 0.7 nm; this suggests that the brushes are somewhat flattened. This shape anisotropy effect raises the question of the specific interactions occurring between (i) brushes of adjacent polymer molecules and (ii) the molecules and the surface, and the relationship between these interactions and the measured height of the molecules. Since the molecules mainly interact with the surface via their densely-packed PS side chains, the height of the molecules reported in this work is expected to be related to the way these exposed PS lateral branches change their orientation towards the surface and interact with it. In this context, stronger interactions would favor the orientation of these branches towards the surface, which would give rise to a lower height of the molecules.

A way to examine the variation of the molecule height as a function of their affinity towards the surface is to modify the hydrophilicity of the substrate. For that purpose, we investigated the surface organization of the deposits on hydrophobic HOPG substrates. In this case, we considered (760/80) copolymer molecules for which an accurate statistical analysis of their conformation and contour length are shown in Fig. 8. Fig. 9a and b show topographic and phase TM–AFM images of a (760/80) copolymer deposit

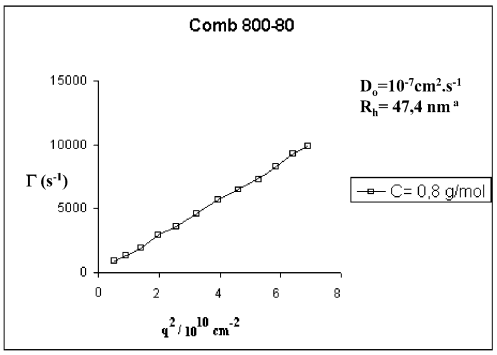

[a]: R_h was calculated from the equation: $R_h = kT/6\pi\eta D_0$ with η the viscosity of THF at 25°C and kT being the thermal energy

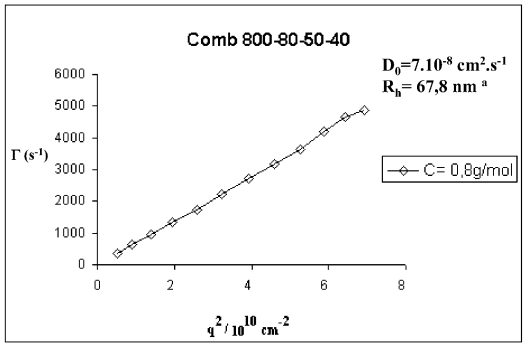

[a]: R_h was calculated from the equation: $R_h = kT/6\pi\eta D_0$ with η the viscosity of THF at 25°C and kT being the thermal energy

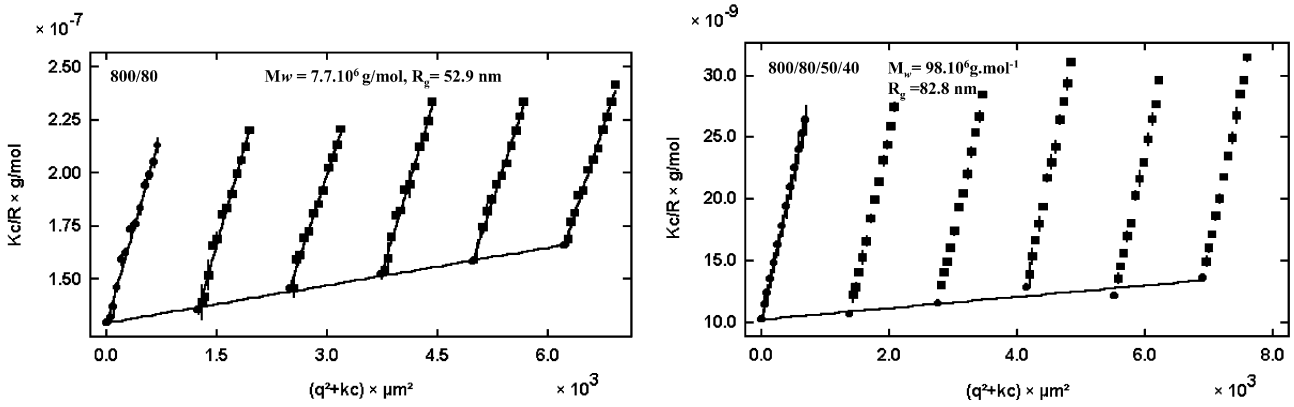

(a) (b)

Fig. 4. (a) Top: angular dependance of Γ ($D = \Gamma/q^2$) of (760/80) in THF at $C = 0.8$ g/ml. Bottom: Zimm plot of (760/80) in THF. (b) Top: angular dependence of Γ ($D = \Gamma/q^2$) of (760/80/50/40) in THF at $C = 0.8$ g/ml. Bottom: Zimm plot of (760/80/50/40) in THF.

on HOPG from a 0.01 wt% solution in THF after a 24 h annealing at 120 °C. Compared to the deposits on mica, for which a heterogeneous multilayered organization is observed, the deposits on HOPG are instead characterized by a morphology that is completely homogeneous on a very large length scale. The morphology appears to consist of a single layer in which a large number of voids can be found. It is likely that the absence of a multilayered organization in these deposits is the direct consequence of the fact that the hydrophobic (PCEVE-*g*-PS) copolymer solution better wets the surface of HOPG. Closer inspection of the morphology nevertheless reveals similarities between deposits on mica and graphite. For instance, one can clearly distinguish individual and elongated molecules densely packed together, as is the case for molecules deposited on mica. However, the average contour length (L_n) and the width of these brush molecules, as determined from TM–AFM images, are evaluated to be 176 and 13 nm, respectively, which fully agrees with the values determined for the molecules on mica. However, on graphite, the molecules are found flattened compared to the deposits on mica, their height being ~3 vs. ~7 nm on mica. We thus observe a change in the volume of the molecules on graphite, their length and width remaining constant. The molecular masses being the same, this means that the internal density of the molecules increases on graphite. We note that all our AFM measurements are carried out using the same tapping parameters and, in particular, the same setpoint-free amplitude ratio [32]. Thus, the observed change in volume of the brushes on graphite cannot be attributed to the squeezing of the material between the tip and the substrate. It most likely originates in the higher affinity of the copolymer PS side chains for graphite, favoring their orientation towards the surface of the substrate and probably a denser packing.

The surface organization and the dimensions of the molecules shown in Fig. 9a and b correspond to regions where the molecules are densely packed, in other words in regions where they are, to a certain extent, constrained by neighboring molecules. In contrast, more isolated molecules can be deposited from more dilute solutions. The corresponding images are shown in Fig. 9c and d. In this case, one can observe molecular assemblies on the surface of graphite. Compared to samples from more concentrated solutions, the molecules are less densely packed within these assemblies and, in a situation of very high dilution (10^{-4} wt%), one can find isolated molecules adopting an elongated conformation on graphite (Fig. 9d). It is worth

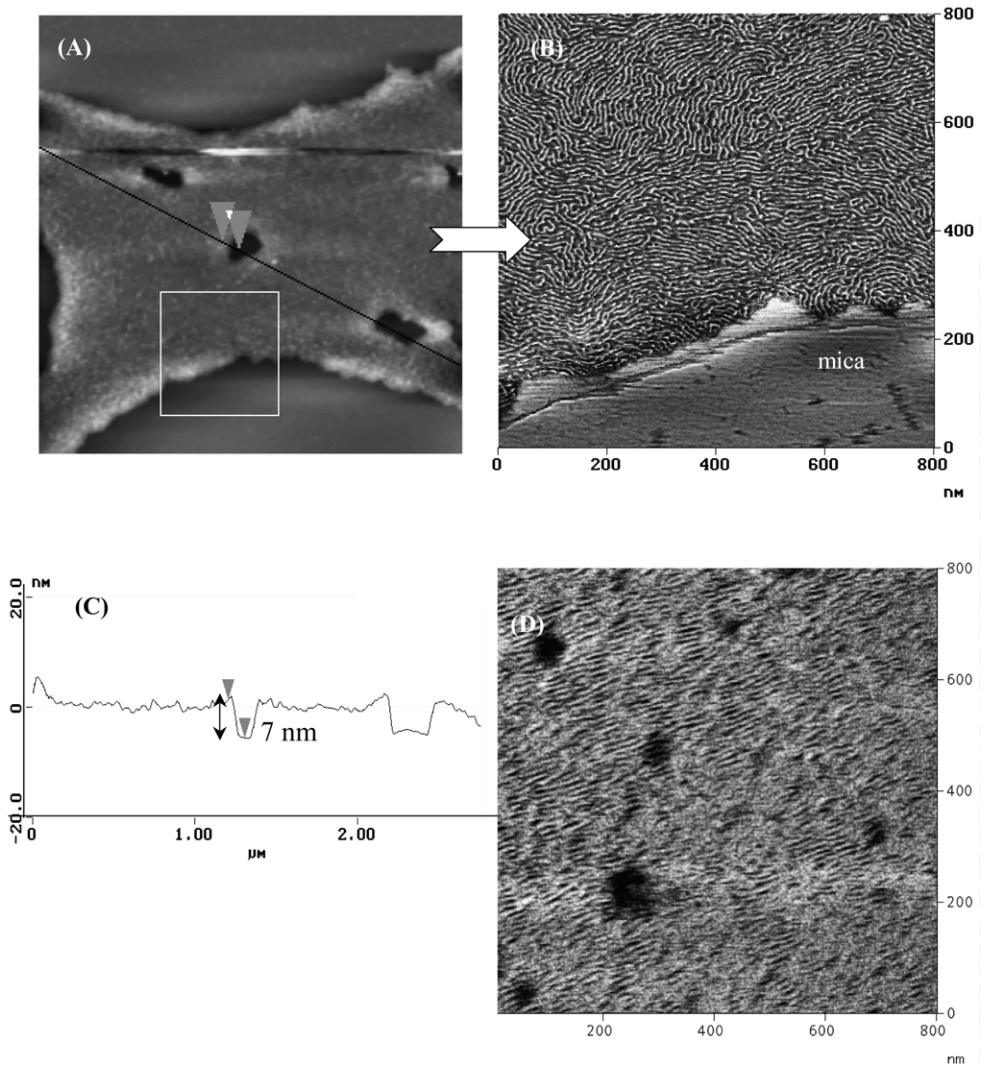

Fig. 5. Top: (A) TM–AFM topographic image ($2.5 \times 2.5\ \mu m^2$) of a monolayer of the (760/80) copolymer (left) and (B) phase image ($800 \times 800\ nm^2$) corresponding to the area defined by the white square (right). Bottom: (C) cross-sectional analysis of the monolayer. (D) surface morphology before thermal annealing at 120 °C.

noting here that this elongated morphology is consistent with the higher affinity of the copolymer molecules towards graphite. Interestingly, the isolated molecules shown in images c and d are much wider than their homologs in the more densely packed assemblies, ~23 vs. 13 nm, respectively. This enlargement is accompanied by a further flattening of the molecules, their height further decreases to an average value of 2 nm. We thus observe here a strong variation of the molecular dimensions (both width and height) depending on the presence of neighboring molecules. In agreement with our previous observations, this flattening is thought to originate from an increasingly efficient orientation of the lateral PS branches towards graphite. When isolated molecules are deposited on graphite, it thus appears that the observed molecular surface organization is largely governed by the strong affinity between the copolymer molecules and graphite. In denser packings, however, molecule–molecule interactions also participate in the surface organization. As a comparison, for the monolayers on mica, molecule–molecule interactions seem to predominate and to determine the surface organization. Various aggregation patterns of the molecules can thus be favored considering the strength of molecule–substrate interactions and the presence (or absence) of neighboring molecules.

The geometrical parameters of the copolymer molecules observed in this work can be compared to the form factors of the same molecules in solution, since the molecular conformation can be deduced from the combination of static and dynamic light scattering measurements. This can be done eitheir in good solvent conditions or preferably in thêta solvent where the thermodynamic properties are dominated by intramolecular interactions. In particular, the ratio of the radius of gyration to the hydrodynamic radius ($\rho = R_g/R_h$) is indicative of the macromolecule form factor. Earlier works have demonstrated that this ratio

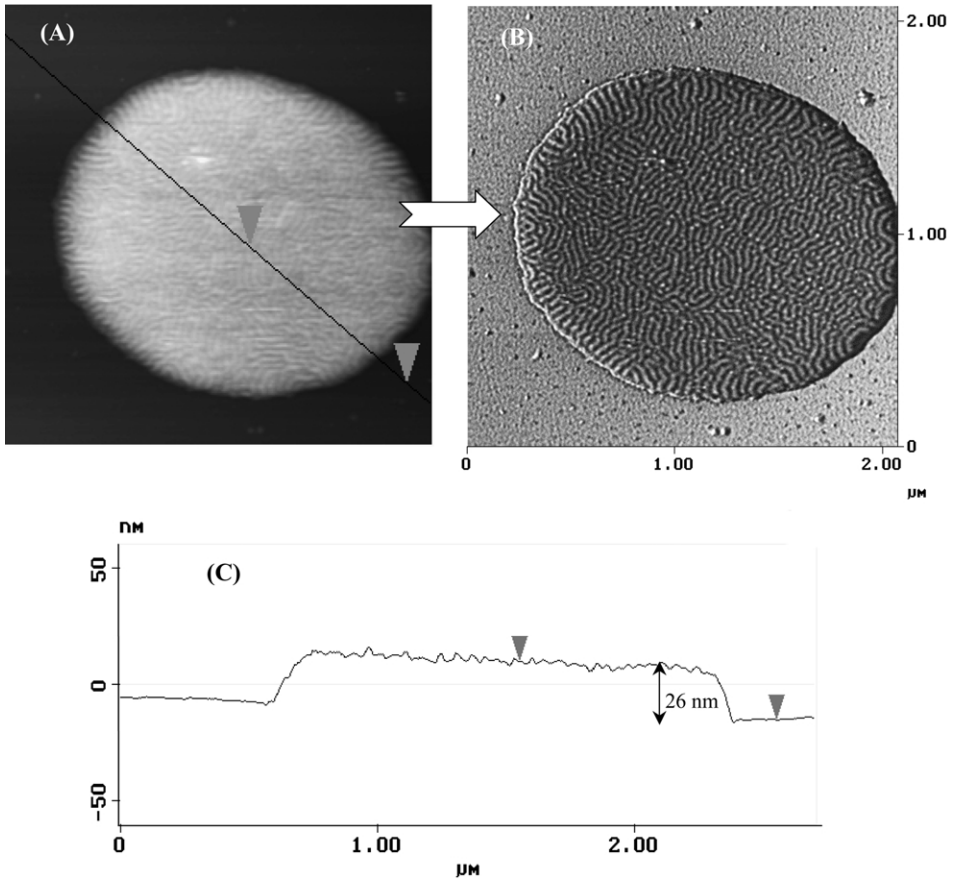

Fig. 6. Top: TM–AFM topographic image ($2.1 \times 2.1\ \mu m^2$) of a monolayer of the (760/80/50/40) copolymer (left) and corresponding phase image (right). Bottom: cross-sectional analysis of the monolayer.

increases for a series of linear (PCEVE-*g*-PS) combs with increasing PCEVE backbone length and identical PS grafts [23]. This evolution is attributed to the change in the form behavior of the molecules from spherical ($\rho = 0.774$) to rodlike or wormlike for stiffer chains ($\rho > 1.1$). Along the same line, the drastic increase of the intrinsic viscosity (η) vs. M_w for $DP_{PCEVE\ backbone} > 50$ units is also a clear signature for the stiffening of the PCEVE-*g*-PS molecules in solution [23]. On that basis, considering a wormlike model for the chains in solution, we can estimate the contour length L of the molecules in solution by mathematically deriving it from the R_g value. In the case of the (760/80) copolymer, this model yields a L value of 183 nm. Although this estimate is rough (because it is derived from a R_g value which usually describes flexible linear chains), it is in very good agreement with the value of the number average molecular length $L_n = 176$ nm determined by AFM for the molecules of the combs within monolayers on mica or in deposits on graphite. In the case of cylinder, the R_g/R_h ratio can be easily calculated from the length L_n and the diameter, d, determined by AFM, using the following equation: $R_g/R_h = 1/\sqrt{3}(\ln(L/d) + 0.38)$ [34]. For the comb (760/80) ($L_n = 176$ nm; $d = 13$ nm) and the hyperbranched polymer (760/80/50/40) ($L_{tot} = 176$ nm; $d = 40$ nm), this yields respectively to $\rho = 1.25$ and 1.15 in good agreement with the R_g/R_h values ($\rho = 1.11$ and 1.22). To go further in the analysis, we would need a more accurate description of the geometrical parameters of the molecules in solution in order to better correlate the solid-state molecular dimensions. A better understanding of their behavior in solution will also help in describing the size evolution of the molecules vs. their molecular architecture in terms of volume and density fluctuations and to relate this evolution to that observed in the AFM images.

4. Conclusions

Studying the surface organization of comb-like and hyperbranched PCEVE-*g*-PS copolymer thin films, we have observed that the degree of lateral ordering of the copolymer chains depends on the intrinsic molecular architecture. In agreement with recent works, we observe that the presence of a large number of densely grafted PS segments onto the PCEVE backbone stiffens the backbone and leads the molecules to adopt a regular brush conformation. The results also indicate that the structural complexity of the lateral side chains strongly affects the size and surface organization of the molecules. In particular, TM–AFM images show that, starting from

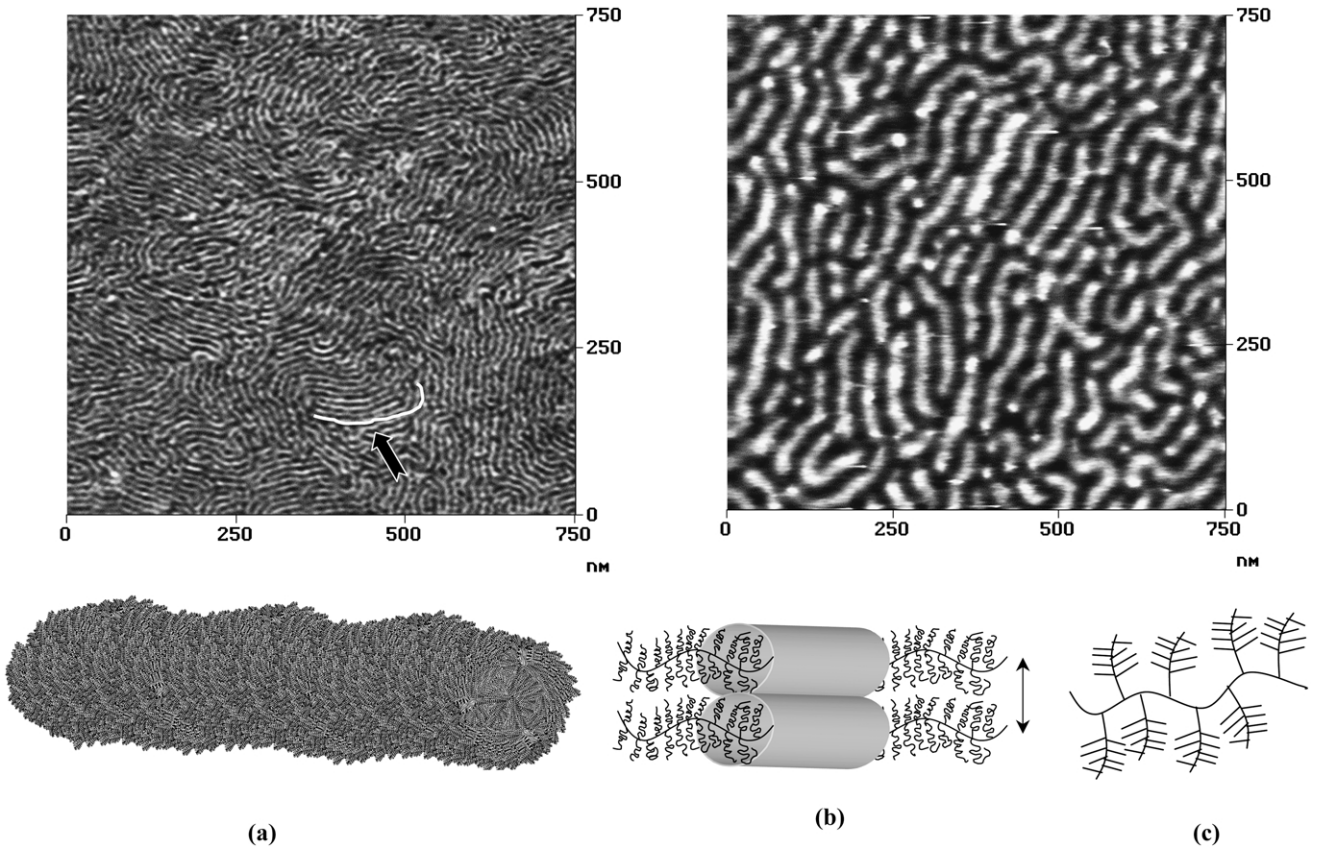

Fig. 7. TM–AFM phase images (750×750 nm^2) of the internal morphology of the (760/80) copolymer monolayer (left) and the (760/80/50/40) copolymer monolayer (right). The left inset (a) shows a schematic view of the corresponding cylindrical brush conformation. The central inset (b) illustrates the intermolecular ordering and the right inset (c) shows a schematic representation of the more complex molecular architecture of the (760/80/50/40) copolymer.

the same backbone, an increase in structural complexity, from a comb-like (PCEVE-*g*-PS) to a hyperbranched (PCEVE-*g*-(PS-*b*-(PCEVE-*g*-PS)) architecture, causes the height and the width of the molecules to increase significantly, while the length of the molecule, as measured with AFM, remains the same.

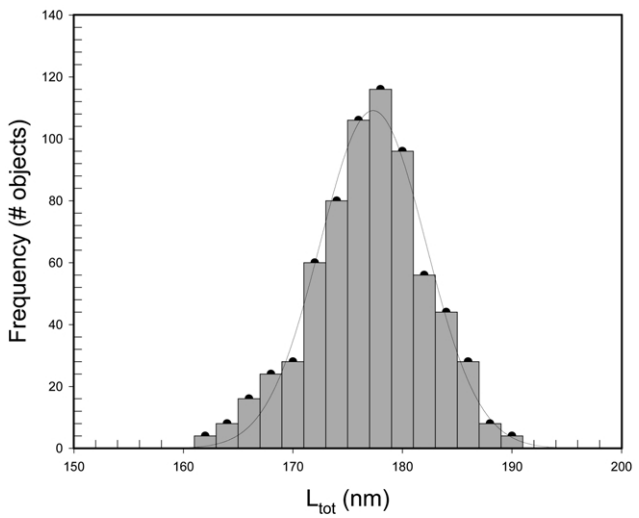

Fig. 8. Molecular length distribution of the (760/80) comb-like copolymer molecules measured by AFM for an ensemble of 678 different molecules. The Gaussian fit yields the values for the number and length average molecular lengths.

In order to study the factors influencing the coiling behavior of the chains, the surface organization of copolymer molecules on graphite was also investigated. The elongated conformation of isolated comb-like copolymer molecules observed in this case is consistent with energetically favored interactions between the PS side chains and the surface of graphite. These interactions favor the PS side chains to preferentially orient along the graphite surface, leading to a stronger shape anisotropy of the molecule. It is important to notice that the geometrical parameters of the molecules and, in particular, their observed contour length on graphite and on mica are in good agreement with data acquired from solution.

Our results show that the copolymer molecules can adopt different surface organizations as a function of their molecular architecture, the nature of the substrate, and the interactions with neighboring molecules. These surface organizations could be exploited to provide specific routes for the fabrication of nanometer-size periodic surfaces with well-controlled morphology. Also, the molecules can be chemically functionalized and designed to develop

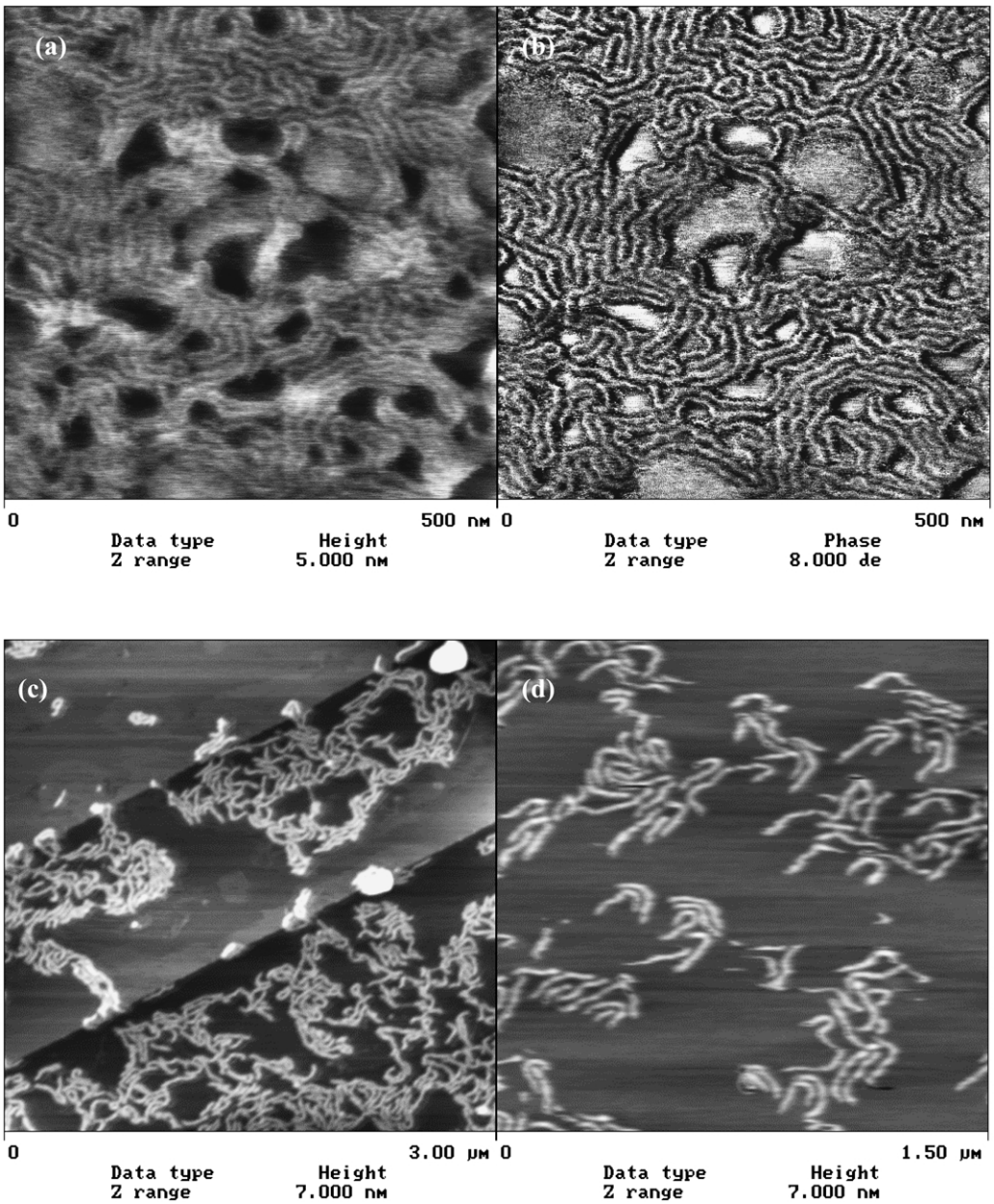

Fig. 9. Top: TM–AFM (500×500 nm^2) topographic and phase images of (760/80) copolymer molecules deposited on graphite from a 0.01 wt% solution in THF and after a 24 h annealing at 120 °C. Bottom: TM–AFM topographic images (3.0×3.0 and 1.5×1.5 μm^2, respectively) of (760/80) copolymer molecules deposited on graphite from a 10^{-4} wt% solution in THF and after a 24 h annealing at 120 °C.

very specific properties. Studies in this direction are in progress.

Acknowledgements

This work was partly supported by the Government of Région Wallonne and the European Commission (Objectif 1-FEDER-Phasing Out) and by the Belgian Federal Government Office of Science Policy (SSTC) 'Pôle d'Attraction Interuniversitaire en Chimie Supramoléculaire et Catalyse Supramoléculaire'. R.L. is Directeur de Recherches du FNRS (Belgium). The Mons-Bordeaux collaboration is supported by the Programme de coopération Tournesol between France and the Communauté Française de Belgique.

References

[1] Weiss PS. Nature 2001;413:585.
[2] Samori P, Francke V, Müllen K, Rabe JP. Chem Eur J 1999;5:2313.
[3] Gunther J, Stupp SI. Langmuir 2001;17:6530.
[4] Ruokolainen J, Saariaho M, Ikkala O, ten Brinke G, Thomas EL, Torkkeli M, Serimaa R. Macromolecules 1999;32:1152.

[5] Sunder A, Mülhaupt R, Haag R, Frey H. Adv Mater 2000;12:235.
[6] Zhai J, Li Y, He Q, Jiang L, Bai FJ. Phys Chem B 2001;105:4094.
[7] Muchtar Z, Schappacher M, Deffieux A. Macromolecules 2001;34: 7595.
[8] Hecht S, Fréchet JM. Angew Chem Int Ed 2001;40:74.
[9] Haag R. Chem Eur J 2001;7:327.
[10] Sunder A, Heinemann J, Frey H. Chem Eur J 2000;6:2499.
[11] Kim YH. J Polym Sci Part A: Polym Chem 1998;36:1685.
[12] Merino S, Brauge L, Caminade AM, Majoral J-P, Taton J-P, Gnanou Y. Chem Eur J 2001;7:3095.
[13] Dziezok P, Sheiko SS, Fischer K, Schmidt M, Möller M. Angew Chem Int Ed Engl 1997;36:2812.
[14] Schappacher M, Bilhaud C, Paulo Ch, Deffieux A. Macromol Chem Phys 1999;200:2377.
[15] Prokhorova SA, Sheiko SS, Mourran A, Azumi R, Beginn U, Zipp G, Ahn C-H, Holerca MN, Percec V, Möller M. Langmuir 2000;16:6862.
[16] Schlüter AD, Rabe JP. Angew Chem Int Ed 2000;39:864.
[17] Krishnamoorti R, Giannelis EP. Langmuir 2001;17:1448.
[18] Tomalia DA, Naylor AM, Goddard WA. Angew Chem 1994;106: 2507.
[19] Fréchet JMJ. Science 1994;263:1710.
[20] Freemantle M. Chem Engng News 1999;6:37.
[21] Deffieux A, Schappacher M. Macromol Symp 1998;45:132.
[22] Deffieux A, Schappacher M. Macromolecules 1999;32:1797.
[23] Deffieux A, Schappacher M. Macromolecules 2000;33:7371.
[24] Prokhorova SA, Sheiko SS, Ahn CH, Percec V, Möller M. Macromolecules 1999;32:2653.
[25] Sheiko SS, Gerle M, Fischer K, Schmidt M, Möller M. Langmuir 1997;13:5368.
[26] Gerle M, Fischer K, Roos S, Müller AHE, Schmidt M, Sheiko SS, Prokhorova SA, Möller M. Macromolecules 1999;32:2629.
[27] (a) Sheiko SS, Möller M. Chem Rev 2001;101:4099. (b) Sheiko SS, Prokhorova SA, Beers KL, Matyjaszewski K, Potemkin II, Khokhlov AR, Möller M. Macromolecules 2001;34:8354.
[28] de Gennes PG. Macromolecules 1980;13:1068.
[29] (a) Zhulina EB, Borisov OV, Pryamitsyn VA, Birshtein TM. Macromolecules 1991;24:140. (b) Subbotin A, Saariaho M, Stepanyan R, Ikkala O, ten Brinke G. Macromolecules 2000;33:6168.
[30] Flikkema E, Subbotin A, ten Brinke G. J Chem Phys 2000;113:7646.
[31] Saariaho M, Subbotin A, Ikkala O, ten Brinke G. Macromol Rapid Commun 2000;21:110.
[32] (a) Zhong Q, Inniss D, Kjoller K, Elings VB. Surf Sci Lett 1993;290: L688. (b) Kopp-Marsaudon S, Leclère Ph, Dubourg F, Lazzaroni R, Aimé JP. Langmuir 2000;16:8432.
[33] (a) Frontali C, Dore E, Ferrauto A, Gratton E. Biopolymers 1979;18: 1353. (b) Balnois E, Stoll S, Wilkinson KJ, Buffle J, Rinaudo M, Milas M. Macromolecules 2000;33:7440.
[34] Antonietti M, Heinz S, Schmidt M, Rosenauer C. Macromolecules 1994;27:3276.
[35] Tao J, Stewart S, Liu G, Yang M. Macromolecules 1997;30:2738.